ISSN 1063-7834, Physics of the Solid State, 2020, Vol. 62, No. 8, pp. 1350–1354. © Pleiades Publishing, Ltd., 2020.
Russian Text © The Author(s), 2020, published in Fizika Tverdogo Tela, 2020, Vol. 62, No. 8, pp. 1204–1208.

MAGNETISM

Magnetic and Resonance Properties of the $Y_{0.5}Sr_{0.5}Cr_{0.5}Mn_{0.5}O_3$ Polycrystal

G. S. Patrin[a, b, *], M. M. Mataev[c], K. Zh. Seitbekova[c], Ya. G. Shiyan[a, b], S. A. Yarikov[a, b], and S. M. Zharkov[a, b]

[a] *Siberian Federal University, Krasnoyarsk, 660041 Russia*
[b] *Kirensky Institute of Physics, Krasnoyarsk Scientific Center, Siberian Branch, Russian Academy of Sciences, Krasnoyarsk, 660036 Russia*
[c] *Kazakh National Women's Teacher Training University, Almaty, 050000 Kazakhstan*
**e-mail: patrin@iph.krasn.ru*

Received April 15, 2020; revised April 15, 2020; accepted April 16, 2020

Abstract—The magnetostatic and magnetic resonance properties of the $Y_{0.5}Sr_{0.5}Cr_{0.5}Mn_{0.5}O_3$ polycrystalline system have been experimentally investigated. The predominance of the intracrystalline ferromagnetic interaction and the antiferromagnetic character of the intercrystallite interaction have been established. The magnetic resonance spectrum in the magnetically ordered region consists of two lines. The high-field line corresponds to the interacting parts of polycrystal shells and the low-field peak is related to the disordered system of ferromagnetic particles.

Keywords: yttrium–strontium chromite manganite, antiferromagnetic interaction, inverse susceptibility, magnetic resonance

DOI: 10.1134/S1063783420080272

1. INTRODUCTION

The compounds belonging to the class of complex oxide materials have been intensively investigated. Complex oxides are attractive for application by their chemical inertness and stability. The creation of materials on the basis of various oxides makes it possible to obtain both purely magnetic and multiferroic compounds [1]. Of great interest are heterogeneous media with the developed interfaces between mesoscopic structural elements, for example, systems with phase stratification, film structures, and nanoscale composites [2]. In this field, the manganite compounds with the general formula $A_xB_{1-x}Mn_yMe_{1-y}O_3$, where A is the rare-earth element, B is, as a rule, the alkaline-earth element, and Me is the 3*d* metal, have been studied most thoroughly [3]. The basic compound is $LaMnO_3$. In particular, doping of this compound with Sr^{2+} ions leads, depending on the impurity concentration, to a rich variety of properties and multiplicity of transitions between different magnetic phases; for instance, at $x = 0.5$, the sample is in the antiferromagnetic phase and exhibits the semiconductor-type conductivity [4]. In the general case, the magnetic and electrical properties of such systems are determined by the ratio between manganese ions Mn^{3+}/Mn^{4+}. On the other hand, in mixed chromite manganites, the effect of exchange bias caused by the competition of exchange interactions between like- and unlike-charged Cr and Mn ions with different valences [5–7] and the effect of the magnetization sign version [8] are observed. The situation becomes even more complicated on the nanoscale. In this case, an additional factor (particle size) for controlling the properties appears; for example, in the $Y_{0.95}Ca_{0.05}MnO_3$ compound, a noticeable change in the permittivity with the nanoparticle size was found [9]. Upon embedding of yttrium impurities instead of lanthanum, the anomalous change in the relative volume, the variation in the inverse susceptibility [10], and the relaxation magnetization processes characteristic of spin glasses [11] are observed. The aforementioned indicates a noticeable effect of yttrium ions on the magnetic properties of manganite crystals. In polycrystalline lanthanum–strontium manganite doped with chromium in low (<8%) concentrations, the reverse spin-glass behavior was observed [12]. In this case, a technique used for sample fabrication strongly affects a set of the properties of polycrystals. Upon transition to the nanoscale, the spatial inhomogeneity inside particles arises and the interparticle interactions are added.

In the literature, there has been a lack of data on the properties of yttrium-based manganites and embedding of chromium ions instead of manganese ions expands the variety of possible exchange interactions. Therefore, we decided to examine the magnetic prop-

erties of polycrystalline yttrium–strontium chromite manganites.

2. EXPERIMENTAL

The $Y_{0.5}Sr_{0.5}Cr_{0.5}Mn_{0.5}O_3$ manganite was synthesized using a mixture of the Y_2O_3, $SrCO_3$, Cr_2O_3, and Mn_2O_3 oxides. The obtained complex oxide samples were prepared by the sol-gel method [13]. The oxides were mixed in the stoichiometric amounts and ground in an agate mortar to obtain a homogeneous mixture. Then, the mixtures were subjected to repeated annealing in a furnace in the temperature range of 600–1100°C with an increase in temperature with a step of 100°C. To improve the homogeneity of the reaction products, the annealing consisted of six stages: 600°C (stage I), 700°C (stage II), 800°C (stage III), 900°C (stage IV), 1000°C (stage V), and 1100°C (stage VI) with a total duration of 39 h. After each synthesis stage, the intermediate grinding was performed. Upon completion of the synthesis, the furnace was switched off and the obtained compound was cooled in the muffle furnace cooling regime.

The phase state of the final products was controlled by X-ray diffraction analysis on a Rigaku Miniflex 600 X-ray diffractometer. The electron microscopy study was carried out on a JEOL JEM-2100 microscope. The magnetic characteristics were studied on an MPMS-XL SQUID magnetometer in fields of up to 50 kOe. The electron magnetic resonance (EMR) spectra were measured on a Bruker E 500 CW EPR spectrometer at a frequency of $\omega_{MWF} = 9.48$ GHz. The resonance measurements were performed in the temperature range of 5–300 K.

3. RESULTS AND DISCUSSION

It was found using X-ray spectroscopy that the crystals have the nominal composition and belong to the orthorhombic syngony with cell parameters of $a = 7.065$ Å, $b = 7.375$ Å, and $c = 6.741$ Å. The average crystallite size can be estimated from the electron microscopy image (Fig. 1), in which one can see a significant crystallite size spread. The local atomic and weight contents of chemical elements determined by transmission spectroscopy are given in Table 1. The data were detected from a spot ~20 nm in diameter (marked in Fig. 1). The spread of the element contents in the sample from one point to another can be 5–6%.

Manganites of different compositions crystallize, as a rule, in the orthorhombic symmetry [3]. In some cases, due to the distortion of the MnO_6 octahedron, the nanophase manganite systems, e.g., $La_{1-x}Me_xMnO_3$ (Me = Ca, Sr [14, 15]) undergo a transition to the monoclinic symmetry. There is the data, however [7], demonstrating that the $La_{0.5}Sr_{0.5}Mn_{0.5}Cr_{0.5}O_3$ polycrystals obtained by the standard solid-state reaction method in air are a mixture of the rhombohedral (42%) and orthorhombic (51%) phases. Magnetically, the samples exhibit, in general, the antiferromagnetic behavior.

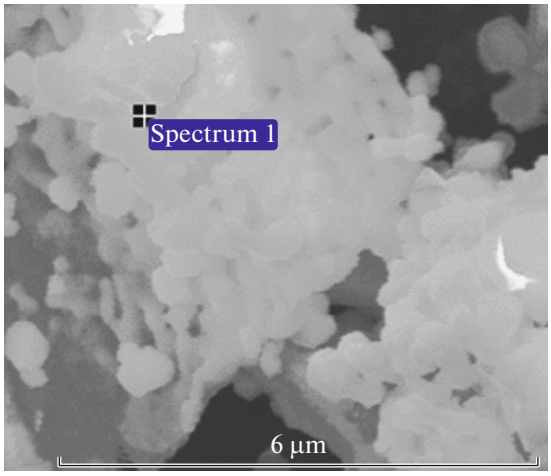

Fig. 1. Electron microscopy image of the polycrystalline $Y_{0.5}Sr_{0.5}Cr_{0.5}Mn_{0.5}O_3$ chromite manganite composition.

The magnetostatic measurements showed that, at low temperatures, the hysteresis magnetization loops are observed. Below 30 K, the hysteresis loop is open (Fig. 2), but the magnetization does not saturate in fields of up to $H \geq 50$ kOe. At temperatures of $T >$ 35 K, the magnetization curve is hysteresis-free and has the form typical of a paramagnet, with the straight slope essentially depending on the measuring temperature (insert in Fig. 2). The shape of the temperature curves of magnetization ($M(T)$) obtained upon sample heating depends on the prehistory or the cooling mode: in nonzero magnetic field (FC) or zero magnetic field (ZFC). Just at a temperature of $T \approx$ 35 K, in the ZFC mode, the $M(T)$ maximum is observed. In fields around 2.5 kOe, a low-temperature magnetization tail arises, the specific weight of which increases with the measuring field. In stronger measuring fields, the maximum is smoothed out and, in fields of $H > 40$ kOe, it is almost absent (Fig. 3). Figure 4 shows temperature dependences of the inverse susceptibility ($1/\chi$) obtained in different magnetic fields (for a standard two-sublattice antiferromagnet [16], we have $\chi = C/(T - \Theta)$, where C is the

Table 1

Element	Weight content, %	Atomic content, %
O	22.3	60.1
Cr	13.7	9.6
Mn	15.53	10.3
Sr	24.53	10.2
Y	23.94	9.8
	100.00	100.00

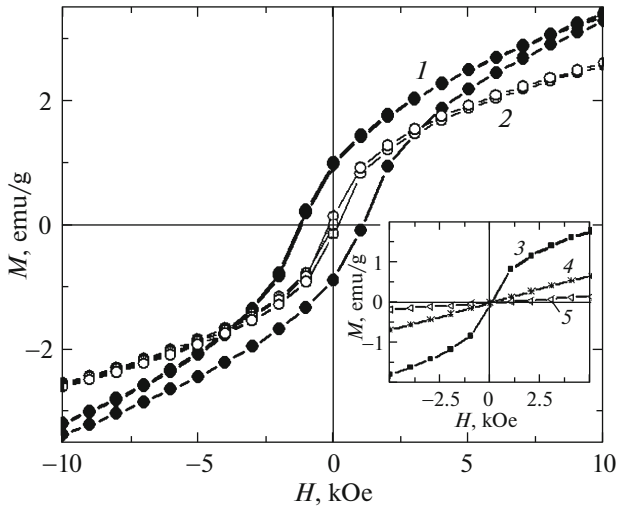

Fig. 2. Field dependences of the magnetization of the $Y_{0.5}Sr_{0.5}Cr_{0.5}Mn_{0.5}O_3$ polycrystal. Curves *1*, *2*, *3*, *4*, and *5* correspond to $T = 4.5$, 25, 35, 75, and 170 K, respectively.

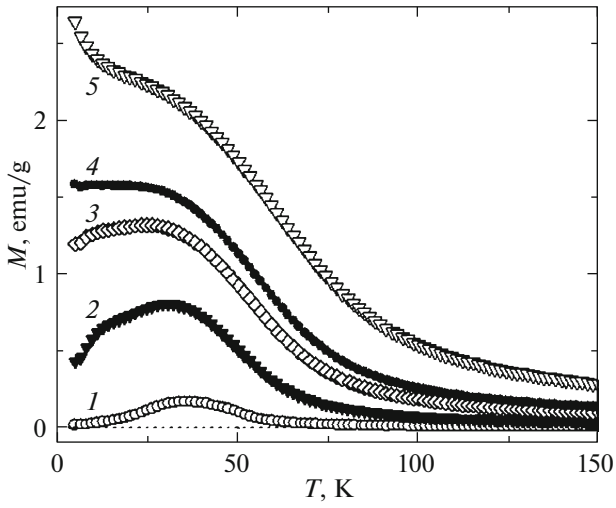

Fig. 3. Temperature dependences of the magnetization for the $Y_{0.5}Sr_{0.5}Cr_{0.5}Mn_{0.5}O_3$ polycrystal. Curves *1*, *2*, *3*, *4*, and *5* correspond to $H = 0.15$, 1.0, 2.5, 3.5, and 7.5 kOe, respectively.

constant, T is the temperature, and Θ is the point of intersection of the asymptote with the abscissa axis, which depends on the ratio between the intra- and interlattice exchanges. In addition, the inset shows the qualitative $1/\chi$ behavior for an antiferromagnet at different magnetic field directions relative to the antiferromagnetic axis. It can be seen that the experimental $1/\chi(T)$ dependence qualitatively corresponds to the antiferromagnetic ordering of a polycrystal [16]. At a measuring field of $H = 2.5$ kOe, the $1/\chi(T)$ curve bending becomes pronounced in the range of $T_N \approx$ 75–90 K, which can be related to the Néel temperature. For all measuring fields, we have $\Theta = -27$ K, while the temperature T_N depends on the measuring field.

Figure 5 shows microwave absorption spectra of the polycrystalline sample at $T = 39$ and 270 K. At temperatures of $T < 80$ K, the spectrum consists of two resonance absorption lines (Fig. 5a) and, in the high-temperature region, one low-field line (line *1*) is observed (Fig. 5b). With increasing temperature, the high-field line significantly decreases in intensity and vanishes near $T \sim 80$ K, which approximately coincides with the T_N region.

The qualitative results can be explained within the model of a two-sublattice antiferromagnet. If $J_1 > 0$ and $J_2 < 0$ are the intra- and interlattice exchange interactions, then, according to [13], we have $\Theta = J_1 + J_2$ and $T_N = J_1 - J_2$. Using the experimental Θ and T_N values, in this case we obtain $J_1 \approx +29$ K and $J_2 \approx -56$ K.

There has been a lack of the literature data on the mixed yttrium chromite manganites and the available data are related to the lanthanum-containing compounds [7, 12, 17, 18]. In the lanthanum–strontium manganites, according to their phase diagram [19], the concentration $x = 0.5$ is intermediate between the ferromagnetic and antiferromagnetic phases. Therefore, embedding of chromium ions and the transition to a mesoscopic crystallite level can shift the boundary of the ferromagnet–antiferromagnet phase transition in either direction.

In single-crystal manganites, the interlattice interaction is, as a rule, noticeably stronger than the intrasublattice interaction [3]. In our case, the average crystallite size is quite large (≈10.3 μm). Here, along with the magnetic order inside crystallites, there is the intercrystallite exchange interaction, which can be

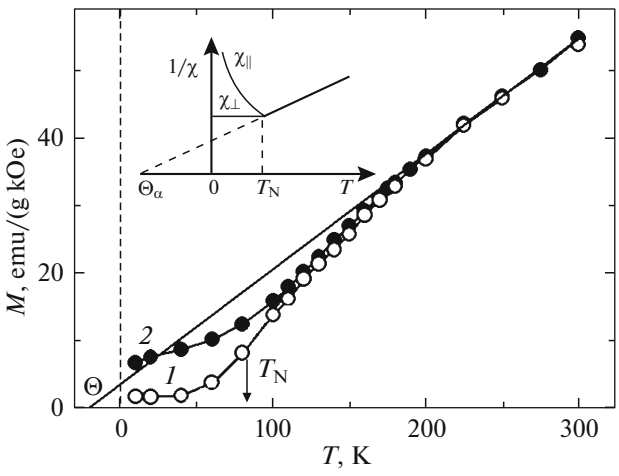

Fig. 4. Temperature dependences of the inverse susceptibility at (*1*) 2.5 and (*2*) 40 kOe. Inset: model dependence for $1/\chi(T)$ from [13].

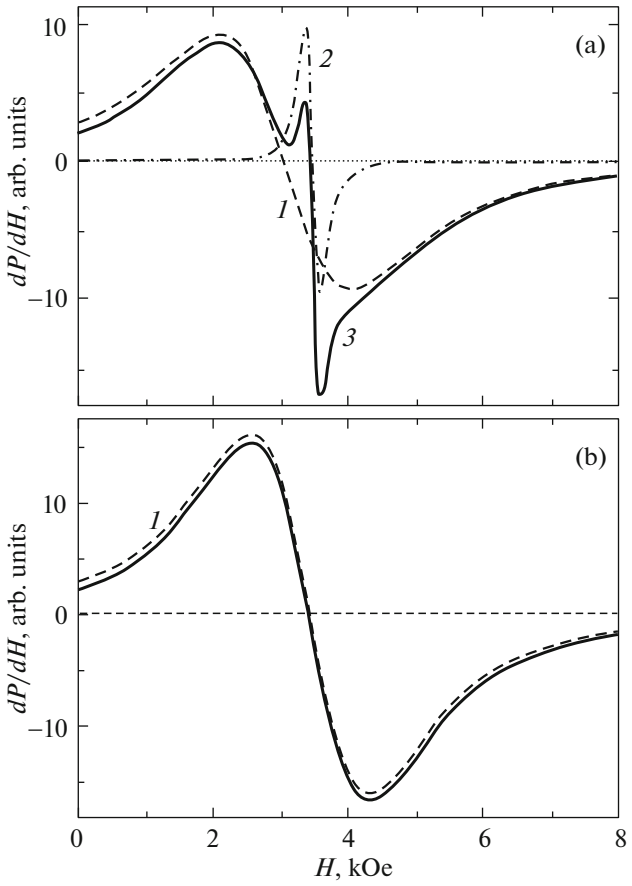

Fig. 5. Resonance absorption spectrum for the $Y_{0.5}Sr_{0.5}Cr_{0.5}Mn_{0.5}O_3$ polycrystal. (a) $T = 39.5$ and (b) 270 K. (*1*, *2*) Fitting by the Lorentz curves and (*3*) experimental curve.

comparable with the exchange inside crystallites; then, the competition of the interactions occurs. The low-temperature magnetization tail in strong magnetic fields is indicative of the presence of a superparamagnetic subsystem and, as was shown in [12], the behavior of the La–Sr–Mn–Cr system with the low Cr content in weak magnetic fields is similar to spin-glass. This gives us grounds to believe that the grains are ferromagnetic and randomly oriented in space, while between the grains the antiferromagnetic interaction occurs. In this case, the intercrystallite exchange interactions should be weaker than the intracrystalline ones. Obviously, in such a system, there is a competition of the intercrystallite interactions. Then, the magnetization in weak magnetic fields $H \le H_{EX}$ (H_{EX} is the intercrystallite interaction exchange field) is determined by the rotation of the magnetic moments of ferromagnetic crystallites and, here, the behavior of the magnetization is similar to spin-glass (curves *1* and *2* in Fig. 3). The behavior in stronger magnetic fields $H > H_{EX}$ is determined by overcoming the intercrystallite antiferromagnetic interactions and rotation of the magnetic moments of crystallites along the external magnetic field direction (curves *3* and *4* in Fig. 3). In strong magnetic fields, the magnetization is related to overcoming the strongest interparticle interactions and intraparticle magnetic anisotropies (curve *5* in Fig. 3).

It is well-known [20] that manganites in the nanoparticle and polycrystalline states have a strong spatial heterogeneity, when the particle's core is surrounded by a surface shell, which, as a rule, has a different composition and may even have a different structure. Then, the ensemble of interacting particles can be presented as a two-phase magnetic system consisting of the internal volume and a shell. The magnetic resonance data show that, at low temperatures, there are two oscillatory modes (Fig. 5a), which indicate the existence of two subsystems. In this case, the low-field resonance peak has an intensity (determined as an area under the corresponding curve) higher by approximately an order of magnitude than that of the high-field peak and a significantly larger linewidth. The approximately resonance fields correspond to the region of 2–3 kOe, which is consistent with the maximum smoothing region in Fig. 3 and the transition to the region of overcoming the antiferromagnetic intercrystallite interactions. Above the transition temperature T_N, the strong-field peak cannot be seen against the background of the low-field peak (Fig. 5b) and the parameters of the low-field peak are almost temperature-independent. These data suggest that the strong-field peak originates from the sample part that is coupled with the polycrystal shell and, when the long-range order vanishes, this part cannot be seen against the low-field peak background. Thus, the low-frequency absorption is related to the resonance from a disordered system of ferromagnetic clusters (crystallites). This is also indicated by the broadening of the observed resonance absorption line. However, to obtain more detailed information about the resonance properties, special investigations are needed.

ACKNOWLEDGMENTS

The magnetic resonance spectra were measured on the equipment of the Krasnoyarsk Territorial Center for Collective Use, Krasnoyarsk Scientific Center, Siberian Branch, Russian Academy of Sciences.

FUNDING

This study was supported by the Ministry of Education and Science of the Republic of Kazakhstan, project no. 05130165 and carried out in the framework of the cooperation agreement between the Siberian Federal University and the Kazakh National Women's Teacher Training University.

CONFLICT OF INTEREST

The authors declare that they have no conflicts of interest.

REFERENCES

1. N. A. Spaldin, S.-W. Cheong, and R. Ramesh, Phys. Today **63**, 38 (2010).
2. *Nanoscale Ferroelectrics and Multiferroics*, Ed. by M. Alguero, J. M. Gregg, and L. Mitoseriu (Wiley, Chichester, UK, 2016), Vol. 1, p. 26.
3. E. Dagotto, in *The Physics of Manganites and Related Compounds* (Springer, Berlin, 2003), Chap. 13.
4. C. Moure and O. Pena, J. Magn. Magn. Mater. **337–338**, 1 (2013).
5. T. Bora and S. Ravi, J. Appl. Phys. **114**, 183902 (2013).
6. C. L. Li, S. Huang, X. X. Li, C. M. Zhu, G. Zerihun, C. Y. Yin, C. L. Lu, and S. L. Yuan, J. Magn. Magn. Mater. **432**, 77 (2017).
7. N. Kallel, M. Hazzez, and N. Ihzaz, J. Supercond. Nov. Magn. **32**, 2623 (2019).
8. A. Kumar and S. M. Yusuf, Phys. Rep. **556**, 1 (2015).
9. N. A. Shah, Appl. Nanosci. **4**, 889 (2014).
10. M. R. Ibarra, P. A. Algarabel, C. Marquina, J. Blasco, and J. García, Phys. Rev. Lett. **75**, 3541 (1995).
11. R. S. Freitas, L. Ghivelder, F. Damay, F. Dias, and L. F. Cohen, Phys. Rev. B **64**, 144404 (2001).
12. J. Dho, W. S. Kim, and N. H. Hur, Phys. Rev. Lett. **89**, 027202 (2002).
13. M. M. Mataev, G. S. Patrin, K. Zh. Seitbekova, Zh. Y. Tursinova, and M. R. Abdraimova, Orient. J. Chem. **35**, 1162 (2019).
14. K. S. Shankar, S. Kar, G. N. Subbanna, and A. K. Raychaudhuri, Solid State Commun. **129**, 479 (2004).
15. J. Dho and S. Ki, J. Phys. Chem. Solids **75**, 1372 (2014).
16. S. Chikazumi, *Physics of Ferromagnetism* (Clarendon, Oxford, 1997), Part 1.
17. O. Cabeza, M. Long, C. Severac, M. A. Bari, C. M. Muirhead, M. G. Francesconi, and C. Greaves, J. Phys.: Condens. Matter **11**, 2569 (1999).
18. C. S. Honga, N. H. Hurb, and Y. N. Choi, Solid State Commun. **133**, 531 (2005).
19. A. Urushibara, Y. Moritomo, T. Arima, A. Asamitsu, G. Kido, and Y. Tokura, Phys. Rev. B **51**, 14103 (1995).
20. V. Markovich, A. Wisniewski, and H. Szymczak, in *Handbook of Magnetic Materials*, Ed. by K. H. J. Bushow (Elsevier, Amsterdam, 2014), Vol. 22, p. 1.

Translated by E. Bondareva